

Electronic Absorption Spectra of Neutral Perylene (C₂₀H₁₂), Terrylene (C₃₀H₁₆), and Quatterylene (C₄₀H₂₀) and their Positive and Negative Ions: Ne Matrix-Isolation Spectroscopy and Time Dependent Density Functional Theory Calculations

Thomas M. Halasinski^{a*}, Jennifer L. Weisman^b, Timothy J. Lee^a, Farid Salama^a and Martin

Head-Gordon^b

^aNASA Ames Research Center

Moffett Field, CA 94035, USA

^bDepartment of Chemistry, University of California, Berkeley

and Chemical Sciences Division, Lawrence Berkeley National Laboratory

Berkeley, CA 94720, USA

Abstract

We present a full experimental and theoretical study of an interesting series of polycyclic aromatic hydrocarbons, the oligorylenes. The absorption spectra of perylene, terrylene and quatterylene in neutral, cationic and anionic charge states are obtained by matrix-isolation spectroscopy in Ne. The experimental spectra are dominated by a bright state that red shifts with growing molecular size. Excitation energies and state symmetry assignments are supported by calculations using time dependent density functional theory methods. These calculations also provide new insight into the observed trends in oscillator strength and excitation energy for the bright states: the oscillator strength per unit mass of carbon increases along the series.

* current address: (please fill in)

I. Introduction

Polycyclic aromatic hydrocarbons (PAHs) are now thought to be ubiquitous throughout the interstellar medium based on the detection of their widespread infrared spectral signature [1]. PAHs are also considered attractive candidates for (some of) the diffuse interstellar bands (DIBs), visible absorption features that are associated with low-density regions of interstellar space [2]. In space, PAH molecules are present as neutral, positively-, and negatively charged species. The charge distribution varies with the physical conditions (interstellar field, electron density and temperature, etc...) that reign in the various regions of the interstellar medium [2]. The comparison of the infrared signatures of PAHs in laboratory spectra with that of the astronomical data suggests that one class of molecules responsible for the interstellar emission features are PAHs. More specific information would result, however, from the detection of the electronic/vibronic signature of interstellar PAHs. Thus, the best prospect in detecting individual PAH molecules in the interstellar medium lies in the identification of the origin of the DIBs.

Current experimental research is directed towards extending the size [3], structure [4], and charge state [5] distributions of the molecules studied in the laboratory. Matrix-isolation spectroscopy experiments offer a crucial guideline for future laboratory studies by allowing the pre-selection of promising PAH molecules to be studied in free jet expansions. Definitive tests of the proposal that PAH ions are responsible for some of the DIBs must await the availability of laboratory measurements of the free molecules and ions in the gas-phase that are still not available for molecules as large as terrylene and quaterrylene presented in this study.

Theoretical calculations are a valuable tool to guide future laboratory studies. Time dependent density functional theory methods [6] are capable of producing reasonably accurate vertical excitation energies and oscillator strengths for large systems. For example, in studies of

naphthalene, perylene and pyrene radical cations [7], we find accuracies of approximately ± 0.3 eV for excitation energies. In addition to simply predicting absorption spectra, it is possible gain insight into the nature of the absorptions and more easily extract trends that may aid in the direction of future investigations. We are able to do exactly this in our current study of perylene, terrylene and quaterrylene.

The collection and analysis of these species provides a spectral database upon which to identify possible candidates for the DIBs, as well as information concerning the photo-physical processes of absorption and emission of radiation within the interstellar medium. It also provides experimental and theoretical information on large polyatomic molecular species that is generally not available from typical molecular spectroscopy studies that traditionally target smaller species. Ultimately, through studies such as this, a more complete understanding of the physical conditions and the chemical evolution within the interstellar medium can be reached.

In a parallel paper [3] we discuss the astrophysical implications of the spectroscopy of a large set of neutral and ionized PAHs. Here, we discuss the detailed analysis of the electronic spectra of a subset of the original set, namely the oligorylenes perylene, terrylene and quaterrylene that presents interesting spectroscopic properties. Matrix-isolated spectra and supporting time dependent density functional theory (TDDFT) calculations are presented for these large molecular systems.

II. Methods

II.a. Experimental

The experimental instrumentation employed in these studies, a UV/visible/NIR spectrometer equipped with its own dedicated sample vacuum chamber and matrix deposition

source, has been previously described [8]. A brief review will be given here. The UV/visible/near-IR instrument is equipped with a sapphire sample window cooled to 4.2 K by an extended liquid helium transfer cryostat. The sample window can be rotated 360° under vacuum to face, alternatively, two spectroscopic window ports, the matrix gas and PAH deposition lines, and a MgF₂ VUV window port.

Single beam spectra of the cold substrate were collected before the matrix was deposited and used as the background for all spectra reported unless noted otherwise. A deuterium lamp provides spectral output from 160-360 nm and a quartz tungsten halogen lamp provides output from 320-2500 nm. Spectra were recorded from 180 to 1000 nm with a nominal resolution of 0.1 nm.

The vaporization and co-deposition of each PAH with the inert gas (neon) was performed using Pyrex tubes (12.7 mm OD) which were mounted on the sample chamber through a stainless steel Cajon Ultratorr fittings and heated from outside the vacuum chamber with the use of heating tape. The tubes were positioned between 4 and 5 cm from the cold window and perpendicular to the surface of the cold substrate. The temperature of the tube was monitored using a chromel/alumel thermocouple mounted on the exterior of each tube with Al foil tape.

Matrix gas was admitted through a port at a position 45° from the plane of the substrate surface and the median between the pyrex tube containing the PAH sample such that the two vapor streams combined before the surface of the window. Typical deposition temperatures for each PAH were 108 °C, 260 °C, and 396 °C for perylene, terrylene, and quaterrylene, respectively. Ne flow rates were estimated to be 12 mmol/h. Based on these flow rates and vaporization temperatures, the matrix/PAH ratio is estimated to be in excess of 1000/1. Typical

deposition times varied from 2 to 4 hrs. Matrices used with NO₂ as an electron acceptor were formed by deposition of premixed 1000/1 Ne/NO₂ gas samples.

A microwave-powered, hydrogen flow (10% H₂/He), discharge lamp (Ophos Instruments MPG 4M) mounted on the MgF₂ vacuum chamber window was used for photolysis of the matrix. This lamp generates nearly monochromatic radiation in the Lyman α line at 121.6 nm (10.2 eV). Typical photolysis times ranged from 2 to 20 minutes.

Perylene (99.5+ %) and NO₂ (99.5+ %) were obtained from Aldrich Chemical Company. The terrylene and quaterrylene samples were obtained from Dr. W. Schmidt (PAH Forschungs Institut, Greifenberg, Germany). Ne (Cryogenic Rare Gas 99.9995%) research grade rare gas was the inert matrix material utilized in the experimental studies. All chemicals were used as received.

II.b. Computational

The ground state structures of perylene, terrylene and quaterrylene were optimized using Kohn-Sham density functional theory (DFT) with the Becke exchange functional [9], LYP correlation functional [10] and the 6-31G* basis set. The neutral, radical cation and radical anion charge states of the three molecules were each optimized at the BLYP/6-31G* level. Time dependent density functional theory (TDDFT) methods were used to determine the absorption spectra of the molecules. The DFT and TDDFT calculations were implemented with the Q-Chem program package [11].

Three basis sets were surveyed to determine the effect of the basis set size on the TDDFT vertical excitation energies of the smallest molecule in this study, perylene. The large size of the terrylene and quaterrylene molecules made it desirable to use the smallest possible basis set for

the calculation of their absorption spectra, without incurring inaccuracies due to insufficient basis size. A difference is generally expected in the basis set dependence for neutral, anionic and cationic excitation energies, and therefore we examined the absorption spectra for each of the three charge states of perylene. Three Pople basis sets were investigated that differed in the presence of polarization and diffuse functions on the heavy atoms. No polarization or diffuse functions were attempted on the hydrogen atoms.

Table 1 shows the basis set effects on the lowest several excitation energies of the neutral, radical cation and radical anion forms of perylene. The vertical excitation energies in electron volts of a given transition are presented next to each other in the table. The neutral and radical anion excitation energies are affected more by the basis set than those of the radical cation. In fact the radical cation absorption energies differ by less than 0.1 eV between the three basis sets. We therefore find BLYP/6-31G//BLYP/6-31G* to be a suitable level of theory for the calculation of the terrylene and quaterrylene radical cation absorption spectra.

The neutral and radical anion excitation energies differ by approximately 0.2 eV or less in going from the basis set with no polarization or diffuse functions, 6-31G, to adding one set of polarization functions, 6-31G*, to additionally adding diffuse functions, 6-31+G*. This difference of 0.2 eV is less than the accuracy of the theory itself, which is about 0.3 eV. And so it is reasonable to settle with the smallest basis set for the neutral and radical anion absorption spectra, and we do this for the neutral species, as for the radical cation. However, one should generally expect diffuse functions to be important for anion excited states, where the negative charge may allow for more diffuse excited states. We therefore find it necessary to calculate the BLYP/6-31+G*//BLYP/6-31G* excitation energies for the terrylene and quaterrylene radical anions.

III. Results and Discussion

III.a. Experimental

The absorption spectra of neutral perylene, terrylene and quaterrylene from 13,000 to 55,000 cm^{-1} (180 – 770 nm) are shown in Figure 1. The most intense and structured absorption band system in all three cases belongs to the electronic transition of the first excited electronic state and shifts to the red as the molecular size increases in the series. Several vibronic bands are observed in the first excited state for all three molecules (expanded views of the 23,000 to 28,000 cm^{-1} (360 – 430 nm) region of the three spectra are shown in Figure 2). The FWHM of the observed vibronic bands also increase with molecular size. Several higher lying excited electronic states are also observed for each molecule. It is not clear if they follow similar trends with molecular size as their spectral assignments are uncertain.

The matrix-isolated samples containing NO_2 -doped Ne were subjected to Lyman alpha (10.2 eV) photolysis. NO_2 was added to the matrix gas to act as an electron acceptor, facilitating the formation of PAH cations by inhibiting the formation of the counter ions (PAH anions). The spectral features which grew upon photolysis for perylene, terrylene, and quaterrylene are shown in the difference spectra in Figures 3A, 4A, and 5A, respectively. A single intense absorption is observed in each case which shifts to the red as the molecular size increases in the series.

The difference spectra of matrix samples photolyzed in the absence of NO_2 for perylene, terrylene, and quaterrylene are given in Figures 3B, 4B, and 5B, respectively. Similar to the spectral features of the PAH cations for this series of molecules, the spectral features of the PAH anions are dominated by a single intense absorption feature which shifts to the red as the molecular size increases in the series. We discuss below each individual spectrum.

III.a.i. Perylene

Several studies of the electronic absorption spectra of perylene isolated in noble gas matrices have been reported previously [12]. The spectral properties are reported here for comparison purposes with the spectra of neutral terrylene and quaterrylene. In addition, we report new calculations for the first excited electronic state. A note should be made at this point concerning the symmetries given for the molecular orbitals and electronic states. The chosen molecular axis, illustrated in Figure 1, has the molecule lying in the xy plane, with x as the long axis of the molecule.

Figure 1A displays the electronic absorption spectrum of neutral perylene from 13,000 to 55,000 cm^{-1} (180 – 770 nm), and Table 2 lists the observed band positions and associated vibrational spacings. The transition from the ground electronic state to the first excited state has been assigned by Joblin et al. [12b], and references therein, to involve a $S_1(B_{1u}) \leftarrow S_0(A_g)$ transition. Using the same molecular axis given in their paper, we assign this transition with $S_1(B_{3u}) \leftarrow S_0(A_g)$ symmetry. Two series of bands were observed for the $S_1(B_{3u}) \leftarrow S_0(A_g)$ transition by Joblin et al. and were assigned as isolated perylene trapped in two different sites in Ne matrices (site a and site b). The full progression of site a is listed in this report, we only list the vibronic origin of site b at 39 cm^{-1} to the red of the vibronic origin of site a.

An expanded view of the 23,000 to 28,000 cm^{-1} (360 – 430 nm) region is illustrated in Figure 2A. While the vibronic progression of the $S_1(B_{3u}) \leftarrow S_0(A_g)$ transition is relatively congested, only a few fundamental vibrational modes (348, 543, 1098, 1293, 1395, and 1601 cm^{-1}) are responsible for the majority of observed vibronic bands. Several spectral features to the blue of the first excited state vibronic progression are also observed in Figure 1 and listed

in Table 2. The tentative assignments given in Table 2 for these features are those of Joblin et al. [12b].

Figure 3A displays the spectral features produced upon photolysis of perylene isolated in a Ne matrix doped with NC_2 and assigned to the perylene cation [7,13]. The position of the observed bands are listed in Table 3 along with assignments from Hirata et al. [7]. The majority of observed bands in the perylene cation show a multicomponent splitting. This splitting has been assigned to the presence of different sites within the solid matrix and/or from transitions involving low vibrational frequencies of the perylene cation [13].

Figure 2B displays the spectral features produced upon photolysis of perylene isolated in a Ne matrix (in the absence of NO_2). The bands which are observed in this spectrum and are absent or very weak in Figure 2A are denoted with an asterisk and assigned to the perylene anion. The position of the observed bands assigned to the perylene anion are listed in Table 4. Multicomponent splitting is observed in the majority of perylene anion bands which are similar in nature to those observed in the perylene cation. Discussion of the assignments for some of the stronger bands is given in section III.b.iii.

III.a.ii. Terrylene

Figure 1B displays the electronic absorption spectrum of neutral terrylene from 13,000 to 55,000 cm^{-1} (180 – 770 nm), and Table 5 lists the observed band positions and associated vibrational spacings. An expanded view of the 23,000 to 28,000 cm^{-1} (360 – 430 nm) region is illustrated in Figure 2B. Similar to the perylene cation, we assign the spectral feature to the red of the main vibronic origin as a site splitting. The larger 154 cm^{-1} shift compared to the 39 cm^{-1} shift of the perylene cation presumably arises from the larger size of the molecular ion. Also

similar to neutral perylene, only a few fundamental vibrational modes (241, 1311, 1398 cm^{-1}) are responsible for the relatively congested vibronic progression observed in the $S_1(B_{3u}) \leftarrow S_0(A_g)$ transition of neutral terrylene. Table 5 also lists tentative assignments of spectral features to transitions involving higher electronic states based on comparison to those spectral features tentatively assigned to the higher electronic states of neutral perylene listed in Table 2.

Figure 4A displays the spectral features produced upon photolysis of terrylene isolated in a Ne matrix doped with NO_2 which we assign to the terrylene cation. The position of the observed bands are listed in Table 6. The majority of observed bands in the terrylene cation show a splitting into multicomponents. We assign the origin of this splitting to a similar site effect responsible for the multicomponents observed in the spectral features for the perylene cation and anion.

Figure 4B displays the spectral features produced upon photolysis of terrylene isolated in a Ne matrix (in the absence of NO_2). The bands which are observed in this spectrum and are absent or very weak in Figure 4A are denoted with an asterisk and assigned to the terrylene anion. The position of the observed bands assigned to the terrylene anion are listed in Table 7. Splitting of the spectral features into multicomponents is also observed in this molecular radical. Discussion of the assignments for some of the stronger bands observed in the spectra of the terrylene cation and anion is given in section III.b.iii.

III.a.iii. Quaterrylene

Figure 1C displays the electronic absorption spectrum of neutral quaterrylene from 13,000 to 55,000 cm^{-1} (180 – 770 nm), and Table 8 lists the observed band positions and associated vibrational spacings. An expanded view of the 23,000 to 28,000 cm^{-1} (360 – 430 nm)

region is illustrated in Figure 2C. Comparison of the spectra in Figures 2A-C show that the observed spectral features appear to broaden with increasing molecular size. While neutral perylene and neutral terrylene both have one spectral feature each which we assign to site splittings, neutral quaterrylene has at least two spectral features lying 89 and 373 cm^{-1} to the red of the most intense transition which may also be assigned to a site effect. Also similar to neutral perylene and terrylene, only a few fundamental vibrational modes (186, 1281, 1395, and 1555 cm^{-1}) are responsible for the relatively congested vibronic progression observed in the $S_1(B_{3u}) \leftarrow S_0(A_g)$ transition of neutral quaterrylene. Table 8 also lists tentative assignments of spectral features to transitions involving higher electronic states based on comparison to those spectral features tentatively assigned to the higher electronic states of neutral perylene (see Table 2) and neutral terrylene (see Table 5).

Figure 5A displays the spectral features produced upon photolysis of quaterrylene isolated in a Ne matrix doped with NO_2 which we assign to the quaterrylene cation. The position of the observed bands are listed in Table 9. Unlike the perylene cation/anion and the terrylene cation/anion, the quaterrylene cation does not exhibit multicomponents to individual spectral bands. Presumably, this is due to the observed increased broadening of the spectral features with molecular size.

Figure 5B displays the spectral features produced upon photolysis of quaterrylene isolated in a Ne matrix (in the absence of NO_2). The bands which are observed in this spectrum and are absent or very weak in Figure 5A are denoted with an asterisk and assigned to the quaterrylene anion. The position of the observed bands assigned to the quaterrylene anion are listed in Table 10. As with the quaterrylene cation, splitting of the spectral features into

multicomponents is not observed. Discussion of the assignments for some of the stronger bands observed in the spectra of the quaterrylene cation and anion is given in section III.b.iii.

At first glance, comparison of the relative spectral intensities for the most intense transition observed for the radical species of perylene, terrylene, and quaterrylene in Figures 3-5 might allow one to conclude that respective transitions increase in intensity with molecular size. However, it is experimentally difficult to quantify the number density of radical cations and radical anions produced upon ionization of the neutral species. Not only is it difficult to measure with some degree of accuracy the number of neutral precursors isolated in a matrix, it is also difficult to quantify the ionization efficiency from experiment to experiment. However, we discuss below a computational argument for the apparent observed increase in relative intensity of the most intense transition with molecular size in the series of molecules studied in this report.

III.b. Computational

The calculated TDDFT absorption spectra for the three molecules in three charge states are presented in Tables 11, 12 and 13, along with the experimental absorptions that may be matched with the TDDFT results. We present the lowest several calculated states for each species. The tables are grouped by molecule, so Table 11 is perylene, followed by terrylene in Table 12, and quaterrylene in Table 13. The vertical TDDFT excitation energies are given in electron volts along with the oscillator strength and symmetry of the transition. Perylene, terrylene and quaterrylene all belong to the D_{2h} molecular symmetry point group and the ground state symmetries of each neutral, radical cation and radical anion are 1A_g , 2A_u and $^2B_{3g}$, respectively. The transition symmetries are assigned on the basis of the molecule lying in the xy plane, with x as the long axis of the molecule.

We will approach the discussion of the computation results in the following manner. We first consider the strong dominant absorption for each molecule in a section on bright states. We discuss the trends observed and explain the origin of these trends. We next consider the astrophysical implications of these bright states in terms of qualitative trends of the excitation energies and oscillator strengths in another section. Finally, we propose possible assignments of states other than the bright states in the last results section.

III.b.i. The Bright States

The experimental absorption spectrum of each molecule is dominated by a strong absorption that is clearly reproduced by theory. Each molecule's strong absorption has B_{3u} transition symmetry, which can be seen in Tables 11-13. The agreement of this strong absorption between experiment and calculation for each radical species is quite good, to within less than one or two tenths of an electron volt. While the neutral calculated results are also qualitatively correct, TDDFT overestimates the strong B_{3u} transition by about one third of an electron volt for each neutral molecule. The neutral strong absorption agreement is not as good as the radical species, however it is within the general accuracy of the method. This phenomenon of better TDDFT performance for radical absorptions than closed shell absorptions merits a more complete study.

The general trend in the strong B_{3u} transition is that the neutral absorption is blue-shifted from the radical cation and radical anion absorption energies for a given molecular backbone. We may understand this energy trend by considering the orbitals involved in the transitions. In order to do this, we have performed attachment/detachment density analysis of the strong absorption for each of the three charge states of perylene. The neutral transition appears to be a

one electron highest occupied molecular orbital (HOMO) to lowest unoccupied molecular orbital (LUMO) excitation, while the radical transitions are combinations of two excitations, with an electron moving into and out of the singly occupied molecular orbital (SOMO). We must look at the attachment/detachment densities and MO plots of the proposed orbitals to confirm the identities of the orbitals involved in the transitions.

Attachment/detachment density plots show the electron density that moves during an electronic excitation [14]. The detachment and attachment densities represent the hole and particle densities, respectively. This analysis identifies which orbitals contribute most to the excitation, through the largest alpha and beta electron eigenvalues of the transition. Next, the density plots may be compared against molecular orbital plots to confirm the orbitals involved in the transition.

Table 14 presents the largest alpha and beta electron eigenvalues for the strong B_{3u} transition attachment/detachment density of the neutral, radical cation and radical anion perylene. The neutral perylene alpha and beta spin largest eigenvalues are identical due to the fact that this is a closed-shell molecule. Since the eigenvalues are approximately a half each, the transition for this molecule is essentially described by a two orbital, one electron picture, where the one electron may be alpha or beta spin. The attachment/detachment density diagram for this transition is shown in Figure 6.

The cation and anion species are both radicals with unrestricted orbitals. This indicates that the SOMO, for example, may not be identical for the alpha and beta electrons. As mentioned earlier, the strong absorption for both of these radicals involves movement into and out of the singly occupied molecular orbital. We therefore need to consider both the alpha and beta attachment/detachment densities separately. The alpha and beta attachment/detachment

densities are shown in Figures 7 and 8 for the radical cation and radical anion, respectively. The fact that there is movement into and out of the SOMO indicates that these transitions are best described by a four orbital, two electron picture.

Molecular orbital diagrams confirm the identities of the orbitals involved in the transitions by comparison with the attachment/detachment density plots. The neutral, radical cation and radical anion molecular orbital diagrams are shown in Figures 9, 10 and 11, respectively. The orbital plots are shown at 0.90 MO contour and the yellow and blue colors denote the different orbital phases.

Figure 9 shows the neutral perylene HOMO (a_u symmetry) and LUMO (b_{3g} symmetry) plots at the BLYP/6-31G//BLYP/6-31G* level. The shape of the HOMO matches the detachment density of the strong absorption, and the LUMO matches the attachment density, Figure 6. Figure 10 reveals that the alpha orbitals involved in the perylene radical cation strong absorption make a SOMO (a_u) to LUMO (b_{3g}) transition. The perylene radical cation beta transition is the third highest occupied molecular orbital (3HOMO, the HOMO of b_{3g} symmetry) to SOMO (a_u). Figure 11 shows the perylene radical anion transition orbitals. The alpha orbital transition is the SOMO (b_{3g}) to the 6th lowest unoccupied molecular orbital (6LUMO, the LUMO of a_u symmetry) and the beta orbital transition is the HOMO (a_u) to SOMO (b_{3g}). These transitions are depicted schematically in Figure 12 and show the relationship of the neutral and radical orbitals, in terms of the orbital symmetries.

The one electron picture for the neutral transition and two electron pictures for the radicals, as shown in Figure 12, explain the experimental blue shift of the neutral strong absorption. The neutral transition, as stated before, is a one-electron HOMO to LUMO excitation, as shown by a single red arrow. The radical transitions involve two electrons,

however not in terms of double excitations, as shown by two different colored arrows. Figure 7 shows alpha and beta electrons being promoted for the radical transitions by arrows in blue and red, respectively. Each red arrow and each blue arrow depicts a one-electron transition from the ground state configuration yielding an excitation of B_{3u} transition symmetry. There is configuration interaction between the one-electron excitations present in the radical transitions that lower their absorption energies from the neutral transition contribution. While TDDFT qualitatively predicts the blue shift for the neutral compounds relative to the cation and anion species, the quantitative accuracy for the shift is in poor agreement with experiment.

III.b.ii. Astrophysical Implications of the Bright States

We may assert some general astrophysical implications of our results based on the observed calculated trends in the bright states. The perylene, terrylene and quaterrylene series of strong B_{3u} transitions show definite trends in the excitation energies and oscillator strengths. The B_{3u} absorption has the same symmetry as the long axis of the molecule, as we will discuss further later, and so we can relate perylene, terrylene and quaterrylene in terms of their long axis.

The trend in excitation energies for all three charge states is that the excitation energy decreases from perylene to terrylene to quaterrylene. And so, as the long axis of the molecule grows, the absorption energy decreases. On the other hand, the oscillator strength increases from perylene to terrylene to quaterrylene. As the molecule size increases the intensity of the absorption does as well. Insight into this phenomenon may be gained by the transition density plots of the strong absorption within a set of charge state derivatives. We investigate the set radical cations as an example of the general behavior of all three groups.

The radical cation transition densities were generated at the BLYP/6-31G//BLYP/6-31G* level. The perylene radical cation transition density is shown in Figure 13, at 0.90 density enclosure. The two transition phases are shown in different colors, yellow as positive and blue as negative. The contours are not opaque and so the darker regions are overlapping phases in one coordinate, although they do not occupy the same spatial density. Figure 13 shows three different views of the same transition density for clarity. It is possible to see from these plots that this transition density is characterized by a dipole moment along the long axis of the molecule.

This transition character is the same for all three radical cations, as seen in Figure 14. This then explains the growing oscillator strength with molecular size. Since the transition dipole is oriented along the long axis of the molecule, the dipole moment increases as the molecule length also increases on that axis. Therefore the intensity of this given absorption grows upon adding naphthalene units to the perylene backbone. We assert that the same type of transition character explains the oscillator strength trends in the neutral and radical anion species as well. This requires that the neutral and radical anion transition densities have the same character as the radical cation transition densities.

The perylene neutral and radical anion transition densities for the strong absorption are shown in Figures 15 and 16, respectively. The top, side and tilted views of the transition density are presented the same way as was done for the perylene radical cation, in Figure 13. The neutral and radical anion species do have the same transition character as the radical cation, and so the growing dipole picture applies to the explanation of growing oscillator strength in each charge state set. We may therefore conclude that in the case of the oligorylene series, larger

species will have stronger absorptions per molecule, stronger absorptions per unit mass of carbon.

The transition density plots suggest a simple model of transition dipole increasing linearly with addition of each naphthalene unit (from perylene to terrylene to quaterrylene) as the long axis length increases. Neglecting changes of excitation energy with increasing size, one would then predict oscillator strength growing quadratically with chain length, and oscillator strength per unit mass of carbon growing linearly with chain length. The calculated results grow slightly less strongly than this (presumably because the above model overestimates charge separation), but it may still be astrophysically significant that oscillator strength per unit mass increases as the oligorylene increases in size.

III.b.iii. Other States

We have so far discussed only the calculated bright state of each molecule in comparison to the experimental spectra. These are the transitions that may be matched with most confidence, since it is clear that the choice must be the calculated absorption with the strongest oscillator strength and appropriate transition symmetry. However it is possible to propose other calculated states as well with some degree of confidence. We may certainly attempt to assign the lowest energy transition, if it has not already been assigned as the strong B_{3u} absorption. It may also be possible to assign transitions directly neighboring the strong absorption or the lowest energy transition, based on the relative oscillator strengths, however these must be asserted with a very low level of confidence, and thus we leave them out.

Tables 11-13, as mentioned earlier, list the calculated TDDFT absorption energies and oscillator strengths of each molecule. The transitions that we propose to assign to experimental

results are indicated by the experimental absorption energy listed next to the corresponding TDDFT result. We do not attempt to assign any states other than the bright state for the neutral species. In each case, the bright state of the neutral molecule is the lowest energy absorption. We do propose additional assignments for the radical cations and radical anions, since the bright state is not the lowest energy absorption.

It is easy to understand why the bright state is not the lowest energy absorption for the radical species, while at the same time it is for the neutral species. Looking back at Figure 12, we recall that the neutral absorption involves a HOMO \rightarrow LUMO transition, which is necessarily the smallest energy gap between orbitals. However, the radical species excitations involve a similar transition as the neutrals, which interacts with another transition that incorporates additional orbitals. These other orbitals are the key to this not being the lowest energy transition for the radical species. The relevant additional orbitals for the cation and anion species are the HOMO and LUMO of appropriate symmetry, respectively. However, these orbitals are not the absolute HOMO and LUMO, they are actually the 3HOMO and 6LUMO. Therefore, excitations that involve the absolute HOMO or LUMO must be lower energy transitions than the bright state transition.

We have assigned the lowest energy transition for each of the radical species. The perylene radical cation and radical anion both have a TDDFT weak B_{2u} symmetry lowest absorption that matches within approximately one tenth of an electron volt with experiment. The lowest energy transitions of the terrylene and quaterylene radical species are all weak B_{3u} symmetry TDDFT absorptions. The calculated terrylene radical results again match well with experiment, to less than one tenth of an electron volt. However, it is interesting that the calculated quaterylene radical results do not have the same level of agreement with experiment.

The TDDFT excitation energies are decreased from the perylene and terrylene energies, in the same way that the bright state decreased in energy with increased molecular size. The experimental results for the quaterrylene radicals, however, show that the lowest transitions are essentially the same energy as for the terrylene radicals.

IV. Conclusions

We have presented experimental and theoretical absorption spectra of perylene, terrylene and quaterrylene and their positive and negative ions. To our knowledge, this is the first matrix-isolation spectroscopy investigation of the larger terrylene and quaterrylene molecules. The oligorylenes isolated in Ne exhibit bright states in the visible region and thus imply possible associations with the diffuse interstellar bands. These matrix-isolation results motivate the further investigation of this subset of PAHs with gas-phase techniques.

Time dependent density functional theory calculations predict absorption spectra in good agreement with the experimental results. The excitation energies and oscillator strengths of the B_{3u} bright states match well, especially for the radical species. The TDDFT investigations have allowed us to understand the character of the bright state transitions. The neutral excitations are shown to be single HOMO \rightarrow LUMO transitions, while the radical excitations are configuration interactions of promotions into and out of the SOMO.

For all neutral and radical species, the B_{3u} transition is the result of a dipole along the long axis of the molecule. TDDFT transition density plots make this visually possible to see, and thus explain the trend in oscillator strengths for this set of oligorylenes. The growth of the molecular backbone along the long axis of the molecule leads to a larger dipole moment for the bright state transition, and thus leads to increasing oscillator strength. It is clear that the strength of the

bright state is stronger per unit mass of carbon for larger oligorylenes, and may indicate a greater significance for these larger systems in relation to the DIBs. Further studies into other medium to large PAH systems are required to determine more general oscillator strength trends.

V. Acknowledgments

JLW and MHG wish to thank the fellow authors for their invitation to collaborate on such an interesting study, and would also like to acknowledge support by the Director, Office of Energy Research, Office of Basic Energy Sciences, Chemical Sciences Division of the US Department of Energy, under Contract No. DE-AC03-76SF00098, and a grant from the Petroleum Research Fund.

VI. References

- [1] (a) Allamandola, L.J.; Tielens, A. G. G. M.; Barker, J. R. *Astrophys. J. Suppl. Ser.* **1989**, 71, 733. (b) Puget, J. L.; Léger, A. *Annu. Rev. Astron. Astrophys.* **1989**, 27, 161. (c) Hudgins, D. M.; Allamandola, L. J. *Astrophys. J. Lett.* **1999**, 513, L69.
- [2] (a) Salama, F.; Bakes, E. L. O.; Allamandola, L. J.; Tielens, A. G. G. M. *Astrophys. J.* **1996**, 458, 621. (b) Salama, F.; Galazutdinov, G. A.; Krelowski, J.; Allamandola, L. J.; Musaev, F. A. *Astrophys. J.* **1999**, 526, 265.
- [3] Ruiterkamp, R.; Halasinski, T.; Salama, F.; Foing, B.; Schmidt, W.; Ehrenfreund, P. Accepted for publication in *Astron. Astrophys.*
- [4] Halasinski, T. M.; Salama, F.; Allamandola, L. J. *Astrophys. J.* In preparation.
- [5] Halasinski, T. M.; Hudgins, D. M.; Salama, F.; Allamandola, L. J.; Bally, T. *J. Phys. Chem.* **2000**, 104, 7484.

- [6] (a) Runge, E.; Gross, E. *Phys. Rev. Lett.* **1984**, 52, 997. (b) Petersilka, M.; Gossmann, U.; Gross, E. *Phys. Rev. Lett.* **1996**, 76, 1212. (c) Bauernschmitt, R.; Alrichs, R. *Chem. Phys. Lett.* **1996**, 256, 454.
- [7] Hirata, S.; Lee, T.; Head-Gordon, M. *J. Chem. Phys.* **1999**, 111, 8904.
- [8] (a) Salama F.; Allamandola, L. J. *J. Chem. Phys.* **1991**, 94, 6964. (b) Salama, F.; Joblin, C.; Allamandola, L. J. *J. Chem. Phys.* **1994**, 101, 10252.
- [9] Becke, A. D. *Phys. Rev. A*, **1988**, 38, 3098.
- [10] Lee, C.; Yang, W.; Parr, R. G. *Phys. Rev. B*, **1988**, 37, 785.
- [11] J. Kong, C. A. White, A. I. Krylov, C. D. Sherrill, R. D. Adamson, T. R. Furlani, M. S. Lee, A. M. Lee, S. R. Gwaltney, T. R. Adams, C. Ochsenfeld, A. T. B. Gilbert, G. S. Kedziora, V. A. Rassolov, D. R. Maurice, N. Nair, Y. Shao, N. A. Besley, P. E. Maslen, J. P. Dombroski, H. Dachsel, W. M. Zhang, P. P. Korambath, J. Baker, E. F. C. Byrd, T. Van Voorhis, M. Oumi, S. Hirata, C. P. Hsu, N. Ishikawa, J. Florian, A. Warshel, B. G. Johnson, P. M. W. Gill, M. Head-Gordon, J. A. Pople, *J. Comp. Chem.* **2000**, 21, 1532.
- [12] (a) Szczepanski, J.; Chapo, C.; Vala, M. *Chem. Phys. Lett.* **1993**, 205, 434. (b) Joblin, C.; Salama, F.; Allamandola, L. *J. Chem. Phys.* **1999**, 110, 7287.
- [13] (a) Joblin, C.; Salama, F.; Allamandola, L. *J. Chem. Phys.* **1995**, 102, 9743. (b) Chillier, X. D. F.; Stone, B. M.; Salama, F.; Allamandola, L. J. *J. Chem. Phys.* **1999**, 111, 449. (c) Hirata, S.; Lee, T. J.; Head-Gordon, M. *J. Chem. Phys.* **1999**, 111, 8904.
- [14] Head-Gordon, M; Grana, A. M.; Maurice, D.; White, C. A. *J. Phys. Chem.*, **1995**, 99, 14261.

VII. List of Figures

- Figure 1. The UV/visible spectra of a co-deposit of (A) a 10 min deposit of perylene in Ne; (B) a 10 min deposit of terrylene in Ne; and (C) a 40 min deposit of quaterylene in Ne. The molecular axis chosen for the symmetries of the molecular orbitals and electronic states of all three PAHs is given in the inset.
- Figure 2. Expanded regions of the spectra shown in Figure 1.
- Figure 3. The visible/near-IR spectra of (A) a 3 h deposit of perylene and NO₂ in Ne followed by 10 min of Lyman α photolysis; (B) a 3 h deposit of perylene in Ne followed by 10 min of Lyman α photolysis. The spectral features denoted with an asterisk have been assigned to the perylene anion.
- Figure 4. The visible/near-IR spectra of (A) a 3 h deposit of terrylene and NO₂ in Ne followed by 10 min of Lyman α photolysis; (B) a 3 h deposit of terrylene in Ne followed by 10 min of Lyman α photolysis. The spectral features denoted with an asterisk have been assigned to the terrylene anion.
- Figure 5. The visible/near-IR spectra of (A) a 3 h deposit of quaterylene and NO₂ in Ne followed by 10 min of Lyman α photolysis; (B) a 3 h deposit of quaterylene in Ne followed by 10 min of Lyman α photolysis. The spectral features denoted with an asterisk have been assigned to the quaterylene anion.
- Figure 6. Neutral perylene BLYP/6-31G//BLYP/6-31G* attachment/detachment density of the $1^1A_g \rightarrow 1^1B_{3u}$ transition at 0.90 density contour.
- Figure 7. Perylene radical cation BLYP/6-31G//BLYP/6-31G* ^{a)} alpha, and ^{b)} beta electron attachment/detachment densities of the $1^2A_u \rightarrow 1^2B_{3g}$ transition at 0.90 density contour.

- Figure 8. Perylene radical anion BLYP/6-31+G*//BLYP/6-31G* ^{a)} alpha, and ^{b)} beta electron attachment/detachment densities of the $1^2B_{3g} \rightarrow 1^2A_u$ transition at 0.90 density contour.
- Figure 9. Neutral perylene BLYP/6-31G//BLYP/6-31G* molecular orbital plots at 0.90 MO contour.
- Figure 10. Perylene radical cation BLYP/6-31G//BLYP/6-31G* ^{a)} alpha, and ^{b)} beta electron molecular orbital plots at 0.90 MO contour.
- Figure 11. Perylene radical anion BLYP/6-31+G*//BLYP/6-31G* ^{a)} alpha, and ^{b)} beta electron molecular orbital plots at 0.90 MO contour.
- Figure 12. Schematic diagram of the neutral, radical cation and radical anion strong B_{3u} transitions.
- Figure 13. Perylene cation BLYP/6-31G//BLYP/6-31G* strong absorption transition density of ^{a)} top view, ^{b)} side view, and ^{c)} tilt view, at 0.90 density contour.
- Figure 14. BLYP/6-31G//BLYP/6-31G* strong absorption transition density of ^{a)} perylene cation, ^{b)} terrylene cation, and ^{c)} quaterylene cation, at 0.90 density contour.
- Figure 15. Neutral perylene BLYP/6-31G//BLYP/6-31G* strong absorption transition density of ^{a)} top view, ^{b)} side view, and ^{c)} tilt view, at 0.90 density contour.
- Figure 16. Perylene anion BLYP/6-31+G*//BLYP/6-31G* strong absorption transition density of ^{a)} top view, ^{b)} side view, and ^{c)} tilt view, at 0.90 density contour.

VIII. List of Tables

- Table 1. Basis set survey of perylene excitation energies.
- Table 2. Vibronic transitions of perylene isolated in Ne.
- Table 3. Vibronic transitions of the perylene cation isolated in Ne.
- Table 4. Vibronic transitions of the perylene anion isolated in Ne.
- Table 5. Vibronic transitions of terrylene isolated in Ne.
- Table 6. Vibronic transitions of the terrylene cation isolated in Ne.
- Table 7. Vibronic transitions of the terrylene anion isolated in Ne.
- Table 8. Vibronic transitions of quaterrylene isolated in Ne.
- Table 9. Vibronic transitions of the quaterrylene cation isolated in Ne.
- Table 10. Vibronic transitions of the quaterrylene anion isolated in Ne.
- Table 11. Perylene calculated TDDFT absorption spectrum.
- Table 12. Terrylene calculated TDDFT absorption spectrum.
- Table 13. Quaterrylene calculated TDDFT absorption spectrum.
- Table 14. Attachment/Detachment density analysis of the $C_{20}H_{12}$ three charge states strong B_{3u} absorption.

Table 1. Basis set survey of perylene excitation energies.

BLYP/6-31G	BLYP/6-31G*	BLYP/6-31+G*
Neutral		
2.6414	2.5826	2.4896
3.6432	3.5832	3.5395
4.3002	4.2122	4.1474
4.9603	4.8461	4.7320
Radical Cation		
1.6246	1.5905	1.5915
1.6831	1.6523	1.6395
1.9174	1.8741	1.8719
2.4389	2.3960	2.3668
Radical Anion		
1.5196	1.4746	1.3930
1.6994	1.6654	1.6065
1.8358	1.7796	1.6399
2.4483	2.4019	2.2555

Excitation energies in eV

BLYP/6-31G* ground state structure

Table 2. Vibronic transitions of perylene isolated in Ne.

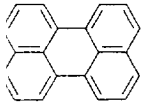
			
C ₂₀ H ₁₂			
Band Position	Band Position	$\Delta\nu$	assignment
419.4	23844	-39	Site b
418.7	23883	0	S₀(A_g)→S₁(B_{3u})
418.1 (sh)	23918	34	(2×17?)
412.7	24231	348	fundamental
(412.1) (sh)	24266	382	(348+34)
(411.5) (sh)	24301	418	(348+2×34)
409.4	24426	543	fundamental
406.8	24582	699	(2×348)
(406.2) (sh)	24618	735	(2×348+34)
(405.5)	24661	777	(429?+348)
(403.6)	24777	894	(543+348)
(401.0)	24938	1054	(3×348)
(400.3)	24981	1098	fundamental
(399.8)	25013	1129	(1098+34)
(397.2)	25176	1293	fundamental
(395.6)	25278	1395	fundamental
(392.4)	25484	1601	fundamental
(391.8)	25523	1640	(1293+348)
*** 390.6	25602	1718	(1369+348)
(390.2)	25628	1744	(1393+348)
(388.9)	25714	1830	(1293+543)
(387.1)	25833	1950	(1601+348)
(384.9)	25981	2097	(1395+2×348)
(384.1)	26035	2151	(1601+543)
(383.6)	26069	2185	(1293+543+348)
(381.9)	26185	2301	(1601+2×348)
(380.5)	26281	2398	(1293+1098)
(379.0)	26385	2502	(1601+543+348)
(377.7)	26476	2593	(2×1293)
376.3	26575	2691	(1395+1293)
(374.9)	26674	2790	(2×1395)
373.4	26781	2897	(1601+1293)
372.0	26882	2998	(1601+1395)
(371.4) (sh)	26925	3042	(1395+1293+348)
(369.1)	27093	3209	(2×1601)
(368.6)	27130	3246	(1601+1293+348)
(367.2)	27233	3350	(1601+1395+348)
(364.5)	27435	3551	(2×1601+348)
(354.9)	28177	4293	(1601+1395+1293)
255.9	34977	0	Ag ?
251.7	35499	521	
274.3	36456	1479	
270.5	36969	1991	(1479+521)
259.8	38491	0	B2g
257.2	38880	389	
243.0	41152	0	B3u
237.4	42123	0	B1u
230.8	43328	1204	Ag ?
221.0	45249	0	B1u
216.1	46275	1026	B3u
213.5	46838	0	B1u

Table 3. Vibronic transitions of the perylene cation isolated in Ne.

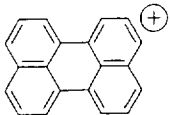
					
$C_{20}H_{12}^+$					
		Band Position	Band Position	Δv	assignment
12582		794.8			
12590	+8	794.3			
12601	+11	793.6	793	~12600	0
12615	+14	792.7			$D_0(^2A_u) \rightarrow D_1(^2B_{2g})$
12631	+16	791.7			
12913		774.4			
12925	+12	773.7			
12942	+15	772.7	773	~12900	~300
12957	+15	771.8			
12970	+13	771.0			
13075		764.8			
13084	+9	764.3			
13098	+14	763.5	763	~13100	~500
13113	+15	762.6			
13130	+17	761.6			
13191		758.1			
13201	+10	757.5			
13222	+21	756.3	757	~13200	~600
13231	+9	755.8			
13328		750.3			
13339	+11	749.7			
13355	+16	748.8	749	~13400	~800
13373	+18	747.8			
		742.1	13475	~875	
		732.4	13653	~1053	
13787		725.3	723	~13800	0
13835	+48	722.8			$D_0(^2A_u) \rightarrow D_1(^2B_{3g})$
		709.8	14088	~288	
		700.4	14277	~477	
		680.6	14692	~892	
		674.9	14817	~792	
		665.7	15021	~933	
		646 (in Argon)	not observed here 15480 argon	0	$D_0(^2A_u) \rightarrow D_1(^2B_{1g})$
		525.3	19036	0	$D_0(^2A_u) \rightarrow D_5(^2B_{3g})$
		329.3	30367	0	$D_0(^2A_u) \rightarrow D_{10}(^2B_{2g})$
		304.2	32873		

Table 4. Vibronic transitions of the perylene anion isolated in Ne.

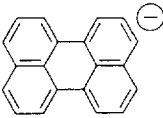
					
\ominus C ₂₀ H ₁₂					
		Band Position	Band Position	Δv	assignment
10293		971.5			
10304	+11	970.5			
10338	+34	967.3	965	10400	0 D ₀ (B _{3g})->D ₁ (B _{2u})
10412	+54	960.4			
10452	+40	956.8			
11471		871.8			
11500	+29	869.6			
11590	+50	862.8	867	11500	1150
11617	+27	860.8			
11715		853.6			
11784	+69	848.6			
11820	+35	846.0	845	11800	0 D ₀ (B _{3g})->D ₃ (B _{2u})
11935	+15	837.9			
12204		819.4			
12276	+72	814.6			
12326	+50	811.3	811	12300	500
12453	+117	803.0			
		556.3	17976	0	D ₀ (B _{3g})->D ₈ (B _{3u})
		320.6	31192		

Table 5. Vibronic transitions of terrylene isolated in Ne.

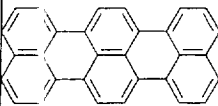
			
$C_{30}H_{16}$			
Band Position	Band Position	Δv	assignment
530.8	18839	-154	Site b
526.5	18993	0	$S_0(A_g) \rightarrow S_1(B_{3u})$
519.9	19234	241	fundamental
513.4	19478	484	(2×241)
507.2	19716	723	(3×241)
500.9	19964	971	(4×241)
492.5	20305	1311	fundamental
490.4	20392	1398	fundamental
484.8	20627	1634	fund. or (1398+241)
479.1	20872	1879	(1398+2×241)
473.6	21115	2121	(1398+3×241)
467.7	21381	2388	(1398+4×241)
462.5	21622	2628	(2×1311)
460.8	21701	2708	(1398+1311)
455.9	21935	2941	(1398+1311+241)
454.2	22017	3023	
450.7	22188	3194	
449.3	22257	3263	
444.5	22497	3504	(3263+241)
325.8	30694	0	
312.2	32031	1337	
296.9	33681	0	
264.0	37879	0	
255.5	39139	0	
247.6	40388	1249	
236.3	42319	0	
228.1	43840	1521	
224.2	44603	0	
217.9	45893	0	

Table 6. Vibronic transitions of the terrylene cation isolated in Ne.

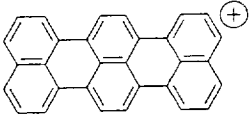
				
$C_{30}H_{16}^+$				
	Band Position	Band Position	Δv	assignment
9158.3	1091.9			
9163.4 +5	1091.3 1090	~9174	0	$D_0(A_g) \rightarrow D_1(B_{3u})$
9192.9 +30	1087.8			
10324	968.6			
10327 +3	968.3 967	~10300	~1126	
10357 +30	965.5			
10490	953.3			
10534 +44	949.3 952	~10500	~1326	
10567	946.3			
10595 +28	943.8 945	~10600	~1426	
10708	933.9			
10712 +4	933.5			
10731 +19	931.9 933	~10700	~1526	
10741 +10	931.0			
10859	920.9			
10891 +32	918.2 920	~10900	~1726	
10929	915.0			
10952 +23	913.1 913	~11000	~1826	
11422	875.5			
11453 +31	873.1			
11481 +29	871.0 871	~11500		
11509 +28	868.9			
11696	855.0			
11729 +33	852.6 854	~11700		?
11867	842.7			
11888 +21	841.2 842	~11900		?
	791.0	12642		?
	780.2	12817		?
	765.7	13060		?
	703.7	14211	0	$D_0(A_g) \rightarrow D_2(B_{2u})$
	690.7	14478	0	$D_0(A_g) \rightarrow D_4(B_{3u})$
	681.2	14680	202	
	674.3	14830	352	
	670.5	14914	436	
	666.2	15011	533	
	664.7	15044	566	
	644.1	15526	1048	
	639.4	15640	1162	
	632.7	15805	1327	
	631.7	15830	1352	
	622.9	16054	1576	
	618.0	16181	1703	
	617.2	16202	1724	
	614.7	16268	1790	
	611.9	16343	1865	
	609.8	16399	1921	

Table 7. Vibronic transitions of the terrylene anion isolated in Ne.

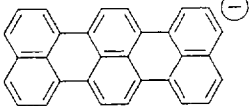
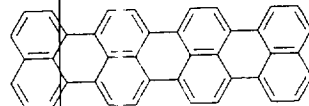
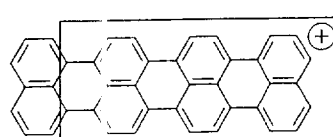
				
\ominus C ₃₀ H ₁₆				
	Band Position	Band Position	$\Delta\nu$	assignment
8851.9	1129.7			
8872.3 +2)	1127.1 1129	8857	0	D ₀ (B _{3g}) \rightarrow D ₁ (B _{3u})
8877.8 +6	1126.4			
	1001.3	9987	1130	
10167	983.6			
10206 +3)	979.8 981	10194		
10225 +1)	978.0			
11069	903.4			
11105 +3)	900.5 902	11100	0	D ₀ (B _{3g}) \rightarrow D ₂ (B _{2u})
	804.6	12429		
	741.5	13486	0	D ₀ (B _{3g}) \rightarrow D ₃ (B _{3u})

Table 8. Vibronic transitions of quaterrylene isolated in Ne.



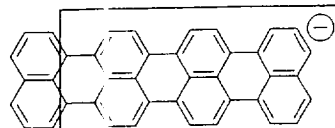
$C_{40}H_{20}$			
Band Position	Band Position	Δv	assignment
621.9	16080	-373	Site c
611.1	16364	-89	Site b
607.8	16453	0	$S_0(A_g) \rightarrow S_1(B_{3u})$
601.0	16639	186	fundamental
594.6	16818	365	(2×186)
588.2	17001	548	(3×186)
582.3	17173	720	(4×186)
575.3	17382	929	(5×186)
565.5	17683	1230	
563.9	17734	1281	fundamental
560.3	17848	1395	fundamental
555.3	18008	1555	fundamental
549.7	18192	1739	
526.7	18986	2533	
524.9	19051	2598	
518.0	19305	2852	
516.3	19369	2916	
513.1	19489	3036	
510.3	19596	3143	
485.2	20610	4157	
478.5	20899	4446	
321.5	31104	0	
316.1	31636	532	
314.1	31837	733	
309.3	32331	1227	
307.8	32489	1385	
306.0	32680	1576	
294.7	33933	2829	
279.2	35817	4713	
269.7	37078	5974	
263.2	37994	0	
252.8	39557	0	
249.6	40064	507	
243.2	41118	0	
240.6	41563	445	
234.6	42626	1508	
226.4	44170	0	
221.4	45167	997	
213.2	46904	2734	

Table 9. Vibronic transitions of the quaterrylene cation isolated in Ne.



$C_{40}H_{20}^{\oplus}$			
Band Position	Band Position	Δv	assignment
1072.6	9323.1	0	$D_0(A_g) \rightarrow D_1(B_{3u})$
1030.6	9703.1		
1016.9	9833.8		
1012.9	9872.6		
990.3	10098		
960.0	10417		
955.8	10462		
942.6	10609		
937.1	10671		
921.3	10854		
910.6	10982		
900.8	11101		
859.4	11636		
835.1	11975	0	$D_0(A_g) \rightarrow D_2(B_{3u})$
807.4	12385		
800.8	12488		
798.3	12527		
776.6	12877		
766.6	13045		
764.8	13075		
760.7	13146		
753.8	13266		
750.9	13317		
738.1	13548		
729.6	13706	0	$D_0(A_g) \rightarrow D_3(B_{3u})$
728.7	13723		
719.9	13891		
718.9	13910		
704.8	14188		
703.8	14209		
694.7	14395		
689.6	14501		
684.1	14618		
679.5	14717		
668.3	14963		
606.2	16496		
665.5	15026		
655.6	15253		
457.1	21877		

Table 10. Vibronic transitions of the quaterrylene anion isolated in Ne.



\ominus $C_{40}H_{20}$			
Band Position	Band Position	Δv	assignment
1106.4	9038.3		
1109.7	9011.4		
1061.5	9420.6	0	$D_0(B_{3g}) \rightarrow D_1(B_{3u})$
1058.7	9445.5		
984.2	10161		
969.5	10315		
946.5	10565		
934.9	10696		
885.7	11291		
880.6	11356	0	$D_0(B_{3g}) \rightarrow D_1(B_{3u})$
861.8	11604		
855.9	11684		
810.1	12344		
805.1	12421		
791.3	12637	0	$D_0(B_{3g}) \rightarrow D_3(B_{2u})$

Table 11. Perylene calculated TDDFT absorption spectrum.

Transition Symmetry	Exc. Energy (eV)	TDDFT Osc. Strength	Expt. Energy (eV)	Expt. Energy (nm)
Neutral				
B _{3u}	2.6414	0.3088	2.96	418.7
B _{2u}	3.6432	0.0047		
B _{2u}	4.3002	0.1015		
B _{3u}	4.9603	0.0293		
B _{3u}	4.9693	0.0025		
Radical Cation				
B _{2u}	1.6246	0.0002	1.56	793.0
B _{3u}	1.6831	0.0001		
B _{2u}	1.9174	0.0288	1.72	722.8
B _{3u}	2.4389	0.3481	2.36	525.3
Radical Anion				
B _{2u}	1.3930	0.0040	1.28	965.0
B _{3u}	1.6065	0.0025		
B _{2u}	1.6399	0.0347	1.47	845.0
B _{1u}	1.7335	0.0028		
B _{3u}	2.2555	0.3328	2.23	556.3

Table 12. Terrylene calculated TDDFT absorption spectrum.

Transition Symmetry	Exc. Energy (eV)	TDDFT Osc. Strength	Expt. Energy (eV)	Expt. Energy (nm)
Neutral				
B _{3u}	2.0211	0.6734	2.36	526.5
B _{2u}	2.9852	0.0001		
B _{2u}	3.3190	0.0075		
B _{2u}	3.4078	0.0046		
B _{3u}	3.8441	0.0116		
Radical Cation				
B _{3u}	1.1723	0.0012	1.14	1090.0
B _{2u}	1.8247	0.0144	1.76	703.7
B _{2u}	1.9143	0.0107		
B _{3u}	1.9257	0.7056	1.80	690.7
Radical Anion				
B _{3u}	1.1026	0.0053	1.10	1129.0
B _{2u}	1.5941	0.0287	1.37	902.0
B _{3u}	1.7626	0.6052	1.67	741.5
B _{2u}	1.8424	0.0038		
B _{1u}	2.0948	0.0030		

Table 13. Quaterylene calculated TDDFT absorption spectrum.

Transition Symmetry	Exc. Energy (eV)	TDDFT Osc. Strength	Expt. Energy (eV)	Expt. Energy (nm)
Neutral				
B _{3u}	1.6730	1.0792	2.04	607.8
B _{3u}	2.9730	0.0118		
B _{2u}	3.1382	0.0038		
B _{2u}	3.2509	0.0093		
B _{2u}	3.4006	0.0012		
Radical Cation				
B _{3u}	0.8930	0.0043	1.16	1072.6
B _{3u}	1.6188	1.0277	1.48	835.1
B _{2u}	1.8067	0.0182	1.70	729.6
B _{2u}	1.9797	0.0027		
Radical Anion				
B _{3u}	0.8370	0.0102	1.17	1061.5
B _{3u}	1.5027	0.9716	1.41	880.6
B _{2u}	1.5565	0.0253	1.57	791.3
B _{2u}	1.6552	0.0004		
B _{2u}	2.1736	0.0034		

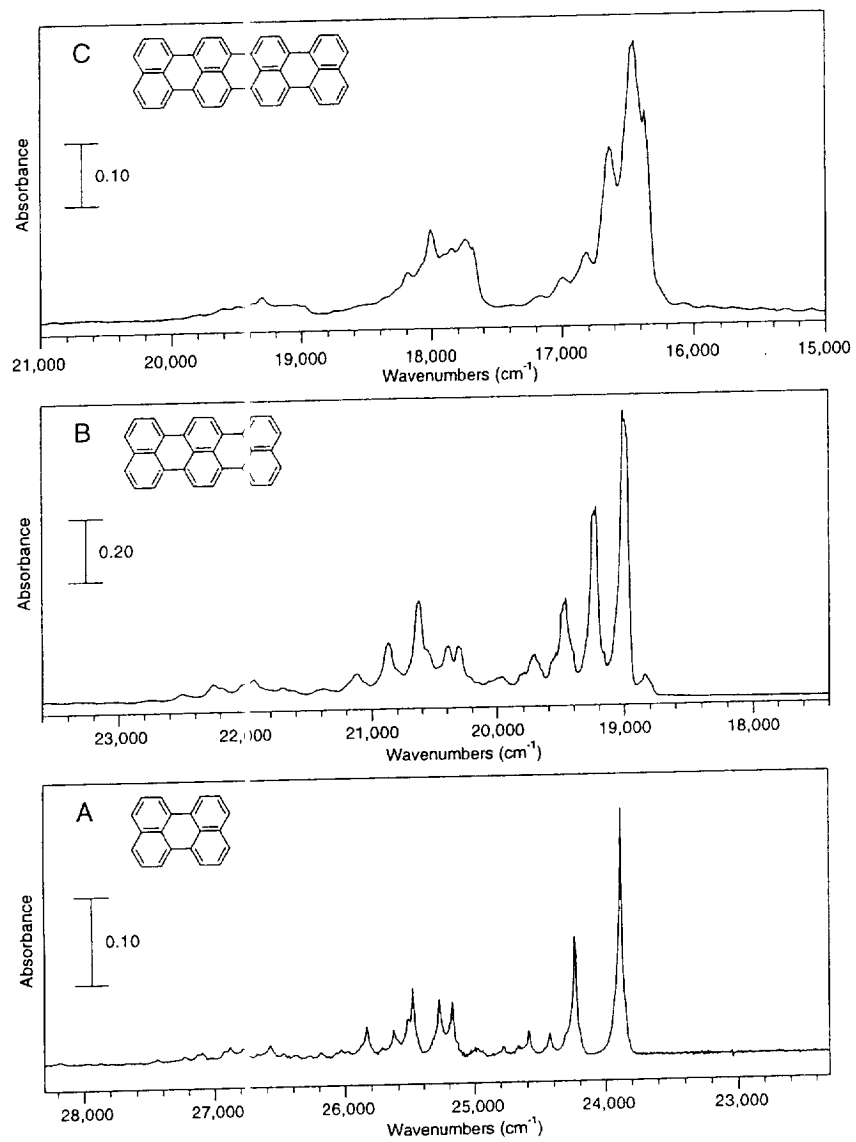
Table 14. Attachment/Detachment density analysis of the C₂₀H₁₂ three charge states

strong B_{3u} absorption.

C ₂₀ H ₁₂ charge state	$\lambda(A)_\alpha$	$\lambda(D)_\alpha$	$\lambda(A)_\beta$	$\lambda(D)_\beta$
neutral	0.492	0.492	0.492	0.492
radical cation	0.443	0.443	0.538	0.538
radical anion	0.644	0.644	0.337	0.337

Largest eigenvalues, λ , are given in units of electronic charge.
Eigenvalues less than 0.1 e are omitted.

B



08/23/00 Abs(07/04)

Figure 2. Expanded regions of the spectra shown in Figure 1.

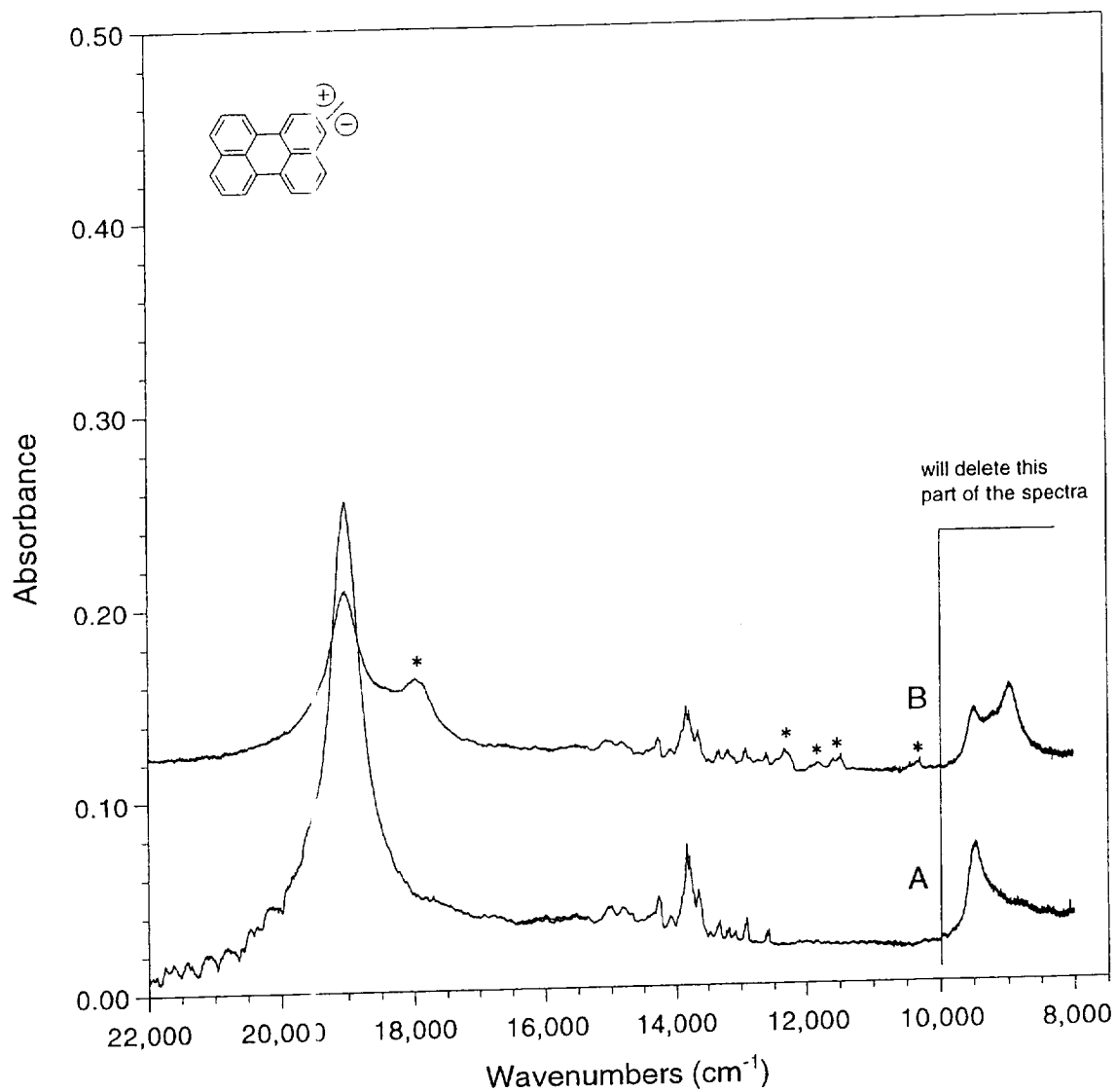


Figure 3. The visible/near-IR spectra of (A) a 3 h deposit of perylene and NO_2 in Ne followed by 10 min of Lyman α photolysis; (B) a 3 h deposit of perylene in Ne followed by 10 min of Lyman α photolysis. The spectral features denoted with an asterisk have been assigned to the perylene anion.

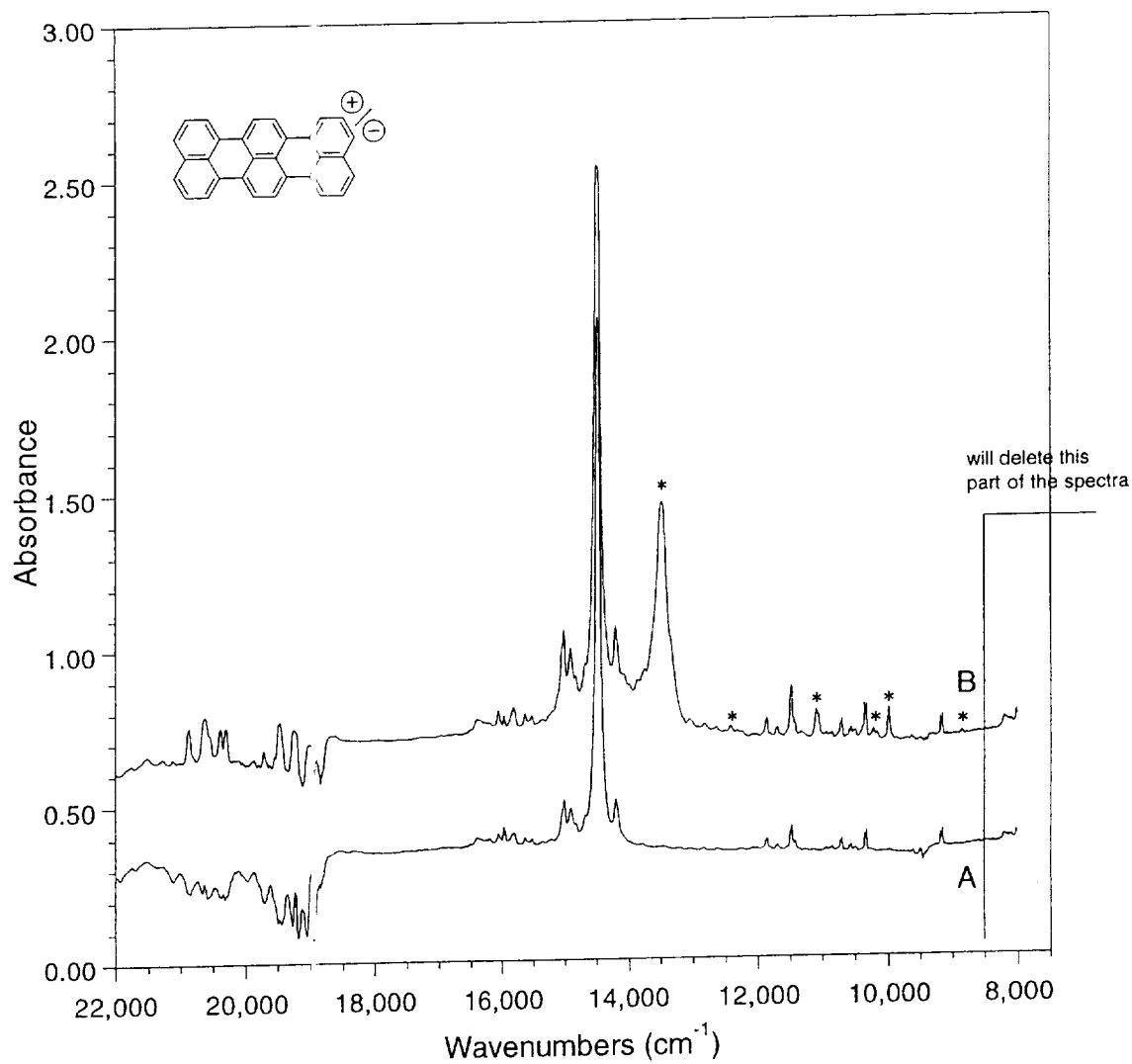


Figure 4. The visible/near-IR spectra of (A) a 3 h deposit of terrylene and NO_2 in Ne followed by 10 min of Lyman α photolysis; (B) a 3 h deposit of terrylene in Ne followed by 10 min of Lyman α photolysis. The spectral features denoted with an asterisk have been assigned to the terrylene anion.

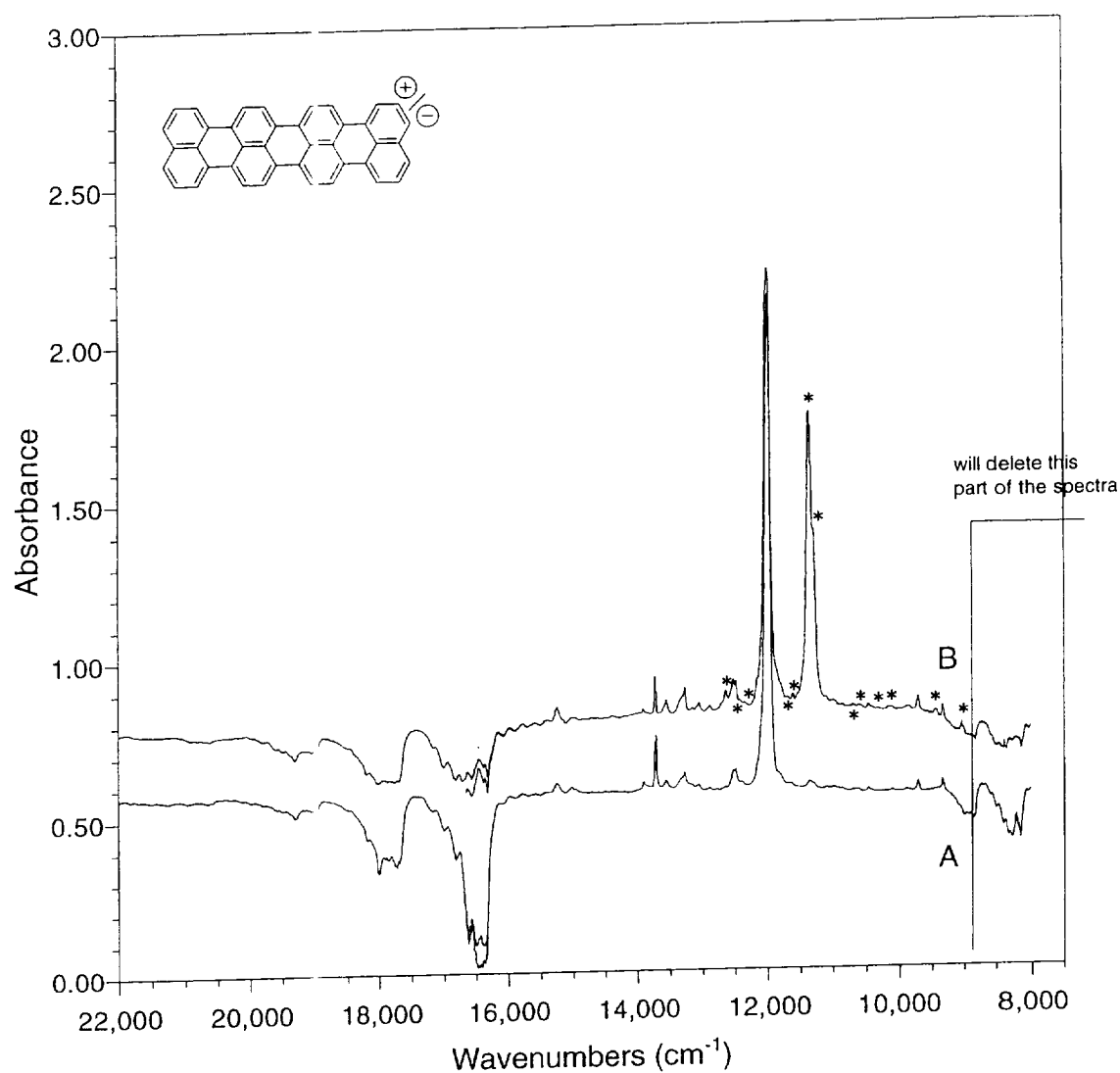


Figure 5. The visible/near-IR spectra of (A) a 3 h deposit of quaterylene and NO_2 in Ne followed by 10 min of Lyman α photolysis; (B) a 3 h deposit of quaterylene in Ne followed by 10 min of Lyman α photolysis. The spectral features denoted with an asterisk have been assigned to the quaterylene anion.

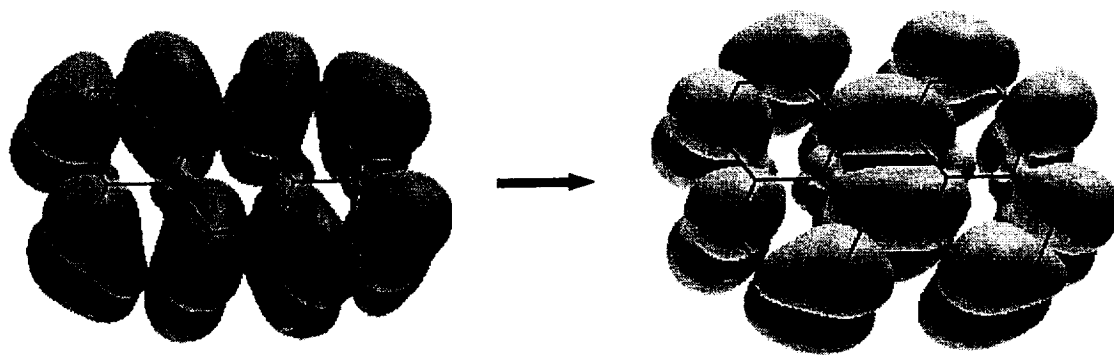
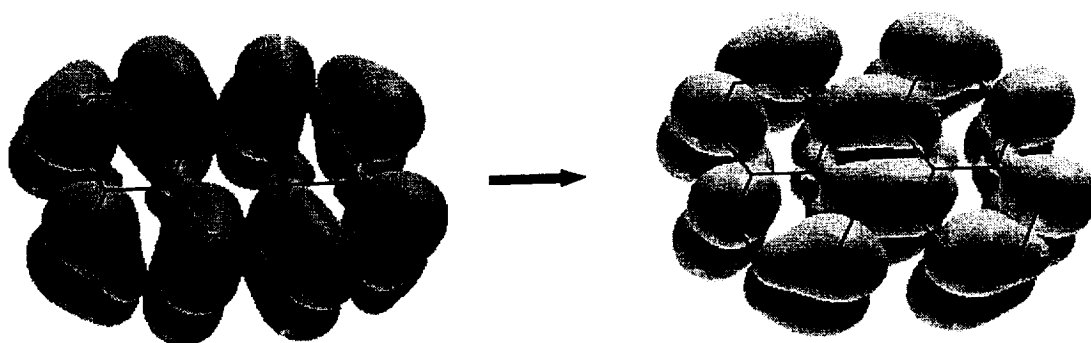


Figure 6. Neutral perylene BLYP/6-31G//BLYP/6-31G* attachment/detachment density of the $1^1A_g \rightarrow 1^1B_{3u}$ transition.

a)



b)

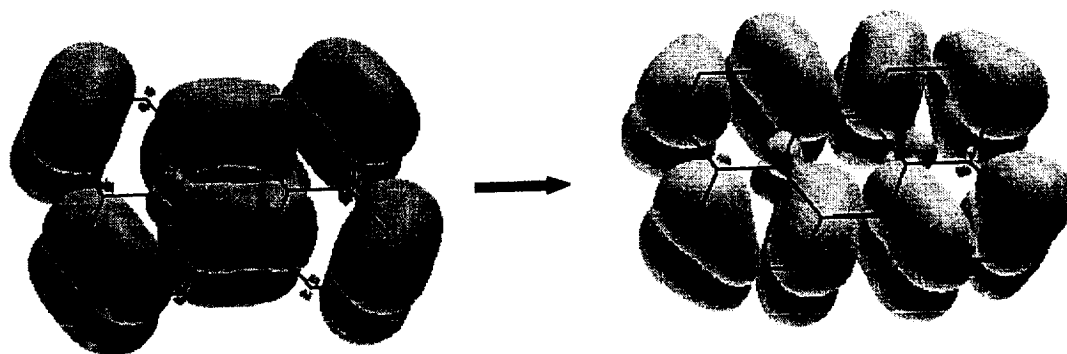


Figure 7. Perylene radical cation BLYP/6-31G//BLYP/6-31G* ^{a)} alpha, and ^{b)} beta electron attachment/detachment densities of the $1^2A_u \rightarrow 1^2B_{3g}$ transition.

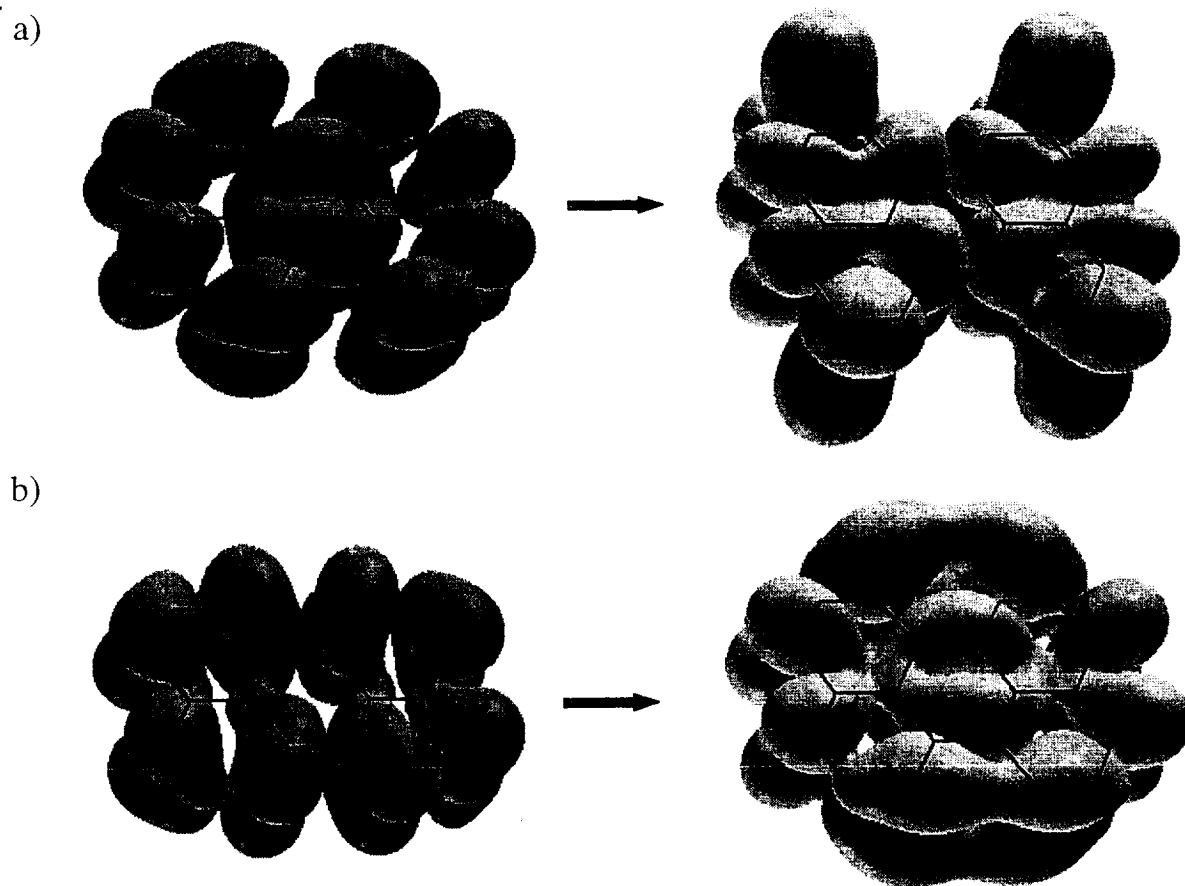
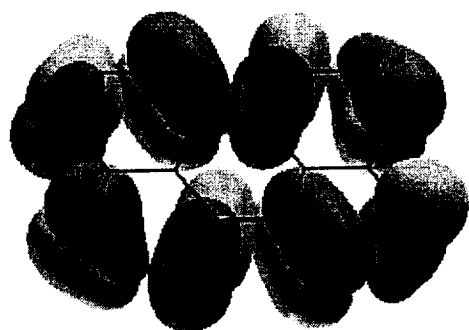
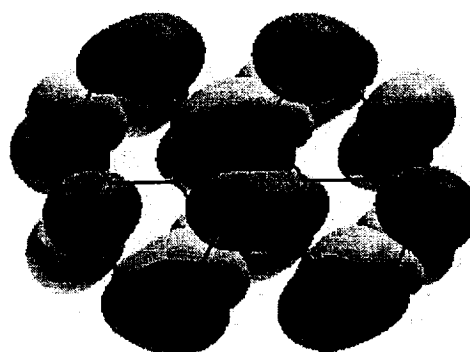


Figure 8. Perylene radical anion BLYP/6-31+G*//BLYP/6-31G* ^{a)} alpha, and ^{b)} beta electron attachment/detachment densities of the $1^2B_{3g} \rightarrow 1^2A_u$ transition.



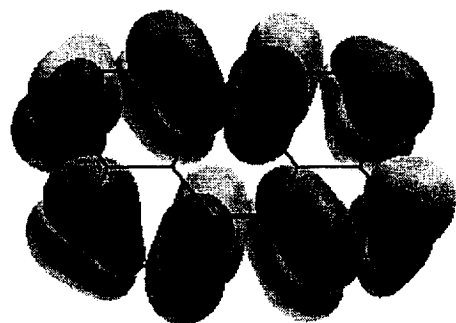
HOMO



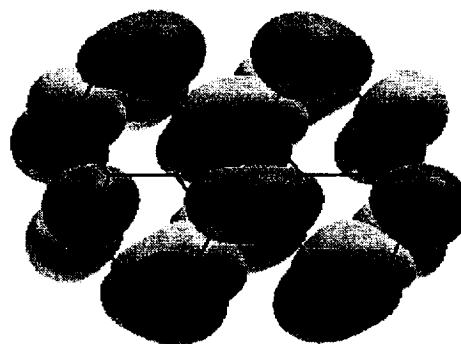
LUMO

Figure 9. Neutral perylene BLYP/6-31G//BLYP/6-31G* squared MO plots of those involved in the $1^1A_g \rightarrow 1^1B_{3u}$ transition.

a)

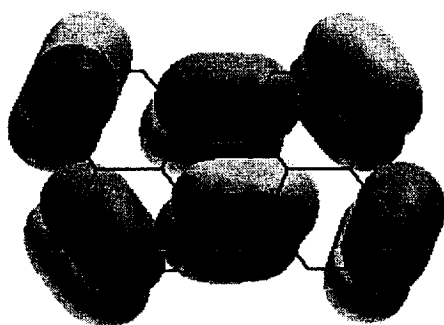


SOMO

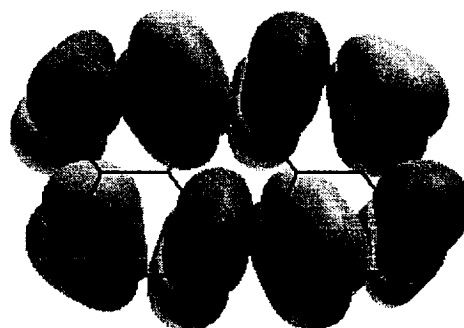


LUMO

b)



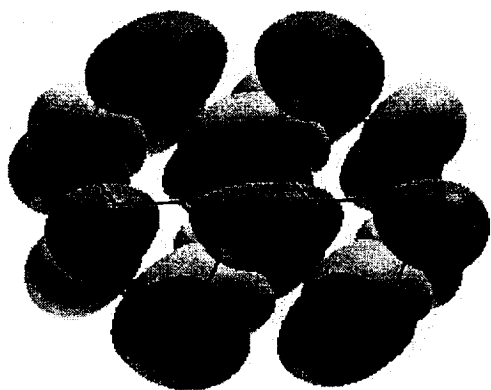
3HOMO



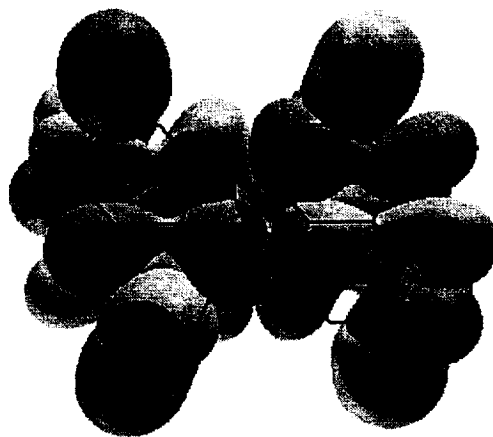
SOMO

Figure 10. Perylene radical cation BLYP/6-31G//BLYP/6-31G* ^{a)} alpha, and ^{b)} beta electron squared MO plots of those involved in the $1^2A_u \rightarrow 1^2B_{3g}$ transition.

a)

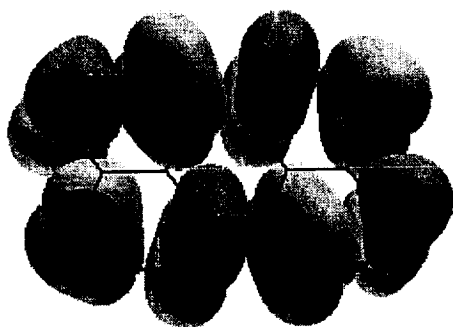


SOMO

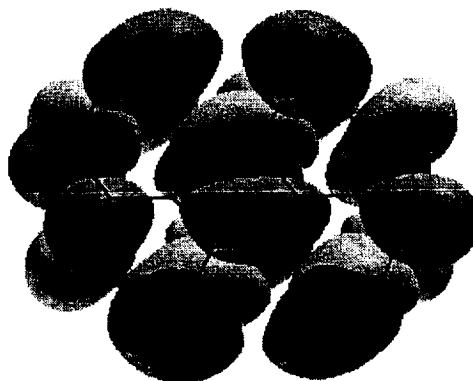


6LUMO

b)



HOMO



SOMO

Figure 11. Perylene radical anion BLYP/6-31+G*//BLYP/6-31G* ^{a)} alpha, and ^{b)} beta electron squared MO plots of those involved in the $1^2B_{3g} \rightarrow 1^2A_u$ transition.

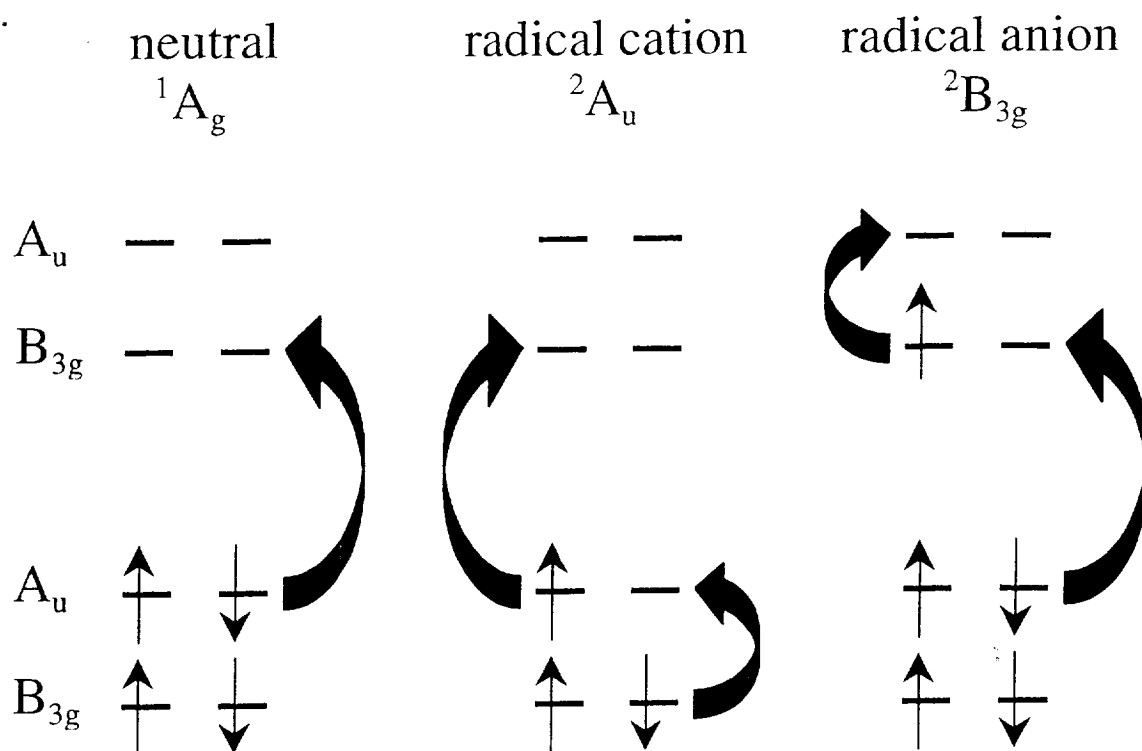
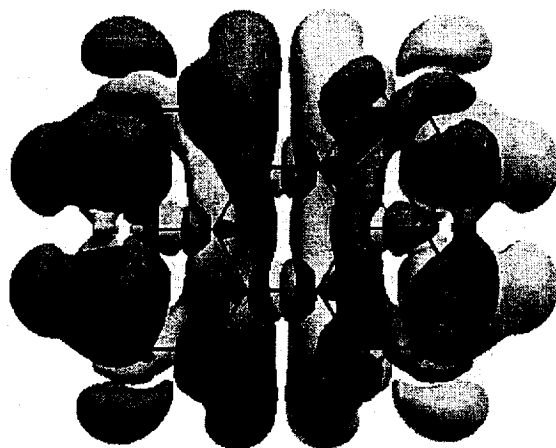
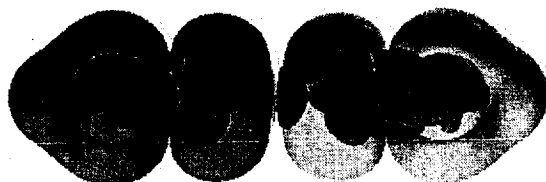


Figure 12. Schematic diagram of the neutral, radical cation and radical anion strong B_{3u} transitions.

a)



b)



c)

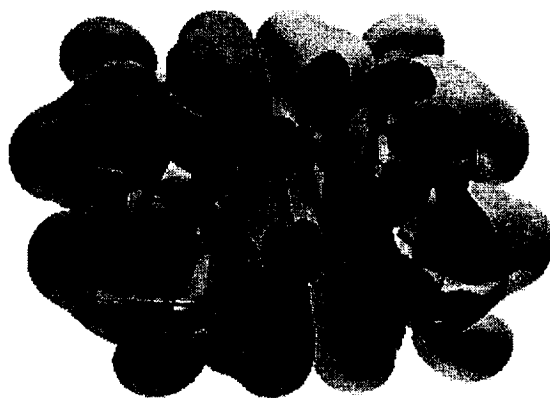


Figure 13. Perylene radical cation BLYP/6-31G//BLYP/6-31G* strong absorption transition density of ^{a)} top view, and ^{b)} side view, and ^{c)} tilt view, at 0.90 density contour.

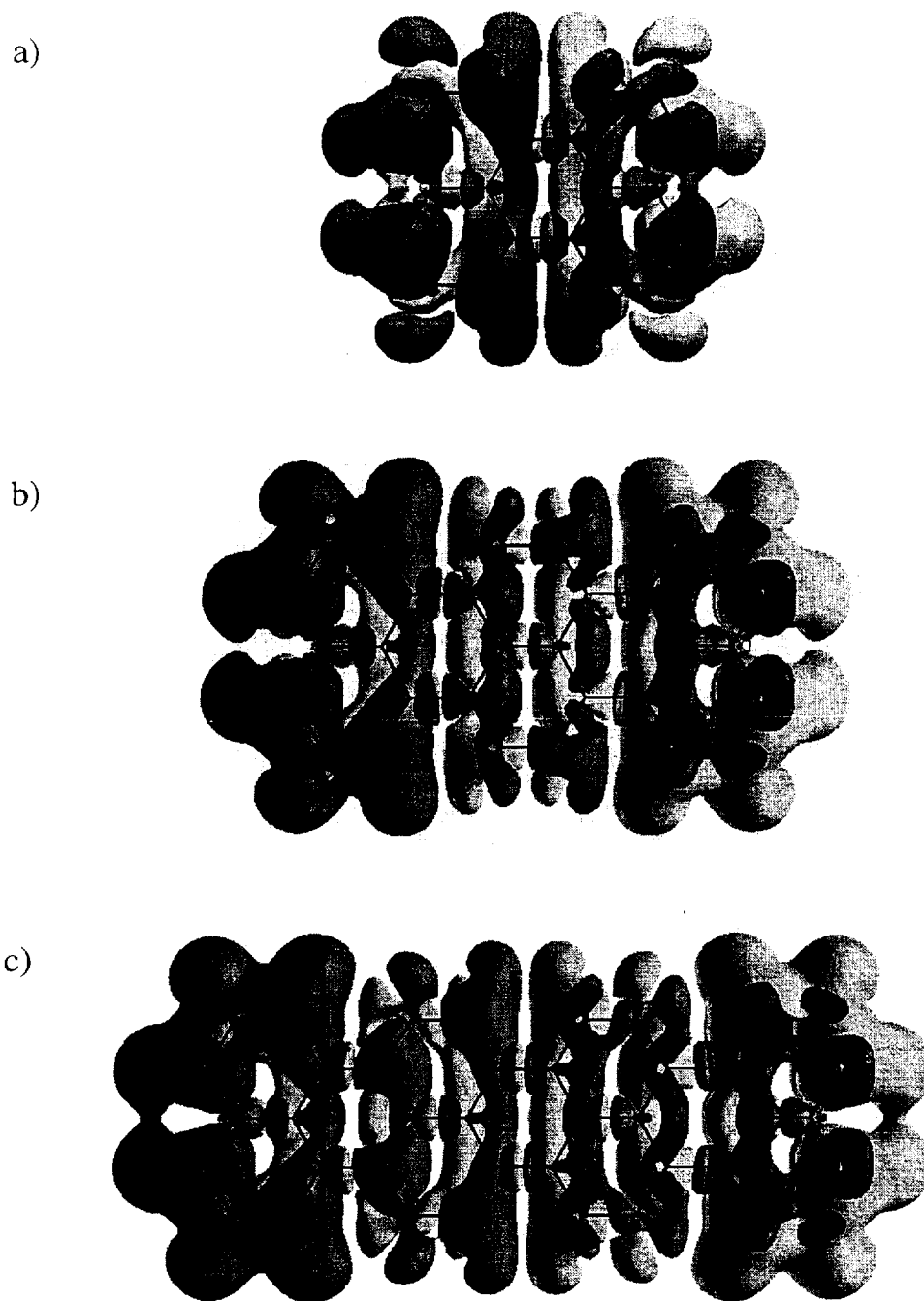
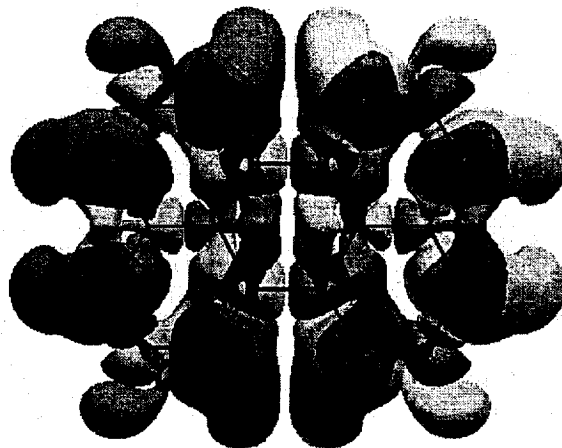


Figure 14. BLYP/6-31G//BLYP/6-31G* strong absorption transition density of ^{a)} perylene cation, and ^{b)} terrylene cation, and ^{c)} quaterrylene cation, at 0.90 density contour.

a)



b)



c)

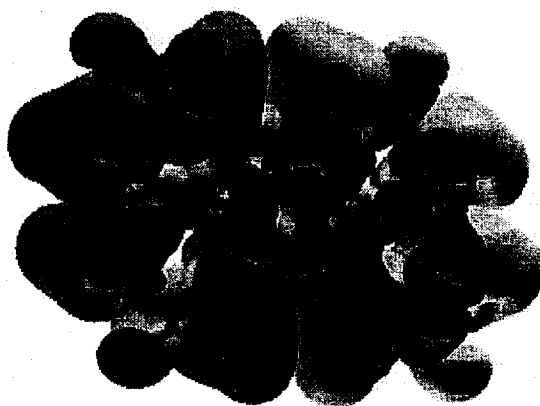
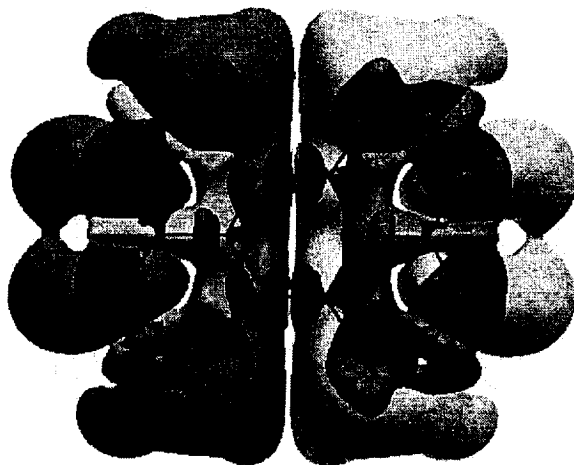
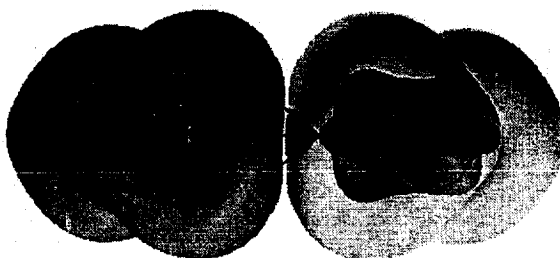


Figure 15. Neutral perylene BLYP/6-31G//BLYP/6-31G* strong absorption transition density of ^{a)} top view, and ^{b)} side view, and ^{c)} tilt view, at 0.90 density contour.

a)



b)



c)

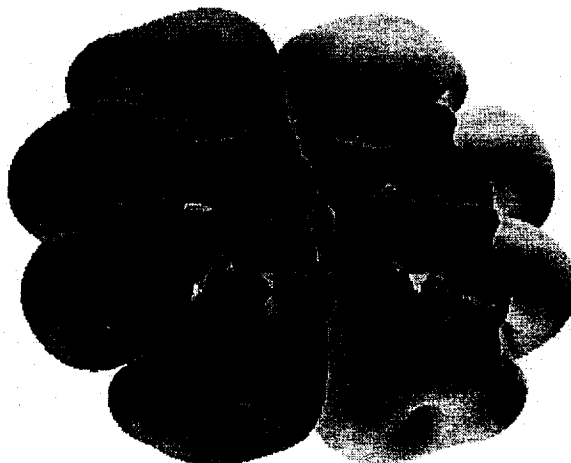


Figure 16. Perylene radical anion BLYP/6-31+G*//BLYP/6-31G* strong absorption transition density of ^{a)} top view, and ^{b)} side view, and ^{c)} tilt view, at 0.90 density contour.